J. Fluid Mech. (2010), *vol.* 651, *pp.* 145–164.
doi:10.1017/S0022112009993879

On condensation-induced waves

WAN CHENG[1], XISHENG LUO[1]† AND M. E. H. VAN DONGEN[2]

[1]Department of Modern Mechanics, University of Science and Technology of China, Hefei 230026, China

[2]Department of Applied Physics, Eindhoven University of Technology, P.O. Box 513, 5600 MB, Eindhoven, The Netherlands

(Received 10 February 2009; revised 2 December 2009; accepted 7 December 2009; first published online 24 March 2010)

Complex wave patterns caused by unsteady heat release due to cloud formation in confined compressible flows are discussed. Two detailed numerical studies of condensation-induced waves are carried out. First, the response of a flow of nitrogen in a slender Laval nozzle to a sudden addition of water vapour at the nozzle entrance is considered. Condensation occurs just downstream of the nozzle throat, which initially leads to upstream- and downstream-moving shocks and an expansion fan downstream of the condensation front. Then, the flow becomes oscillatory and the expansion fan disappears, while upstream and much weaker downstream shocks are repeatedly generated. For a lower initial humidity, only a downstream starting shock is formed and a steady flow is established. Second, homogeneous condensation in an unsteady expansion fan in humid nitrogen is considered. In the initial phase, two condensation-induced shocks are found, moving upstream and downstream. The upstream-moving shock changes the shape of the expansion fan and has a strong influence on the condensation process itself. It is even quenching the nucleation process locally, which leads to a renewed condensation process more downstream. This process is repeated with asymptotically decreasing strength. The repeated interaction of the condensation-induced shocks with the main expansion wave leads to a distortion of the expansion wave towards its shape that can be expected on the basis of phase equilibrium, i.e. a self-similar wave structure consisting of dry part, a plateau of constant state and a wet part. The strengths of the condensation-induced waves, as well for the Laval nozzle flow as for the expansion fan, appear to be in qualitative agreement with the results from the analytical Rayleigh–Bartlmä model.

1. Introduction

Humid air brought in a supersaturated state will tend to restore equilibrium by means of nucleation and condensation. The latter process refers to the growth of droplets that already exist. Nucleation is the formation of the smallest stable droplets possible and can be either heterogeneous or homogeneous. In heterogeneous nucleation, solid particles facilitate the formation of nuclei and the number density of droplets is determined by the concentration of these foreign nuclei. In homogeneous nucleation, the droplets are formed by a spontaneous clustering of vapour molecules and both number density and size of the droplets strongly depend on the time history of the humid mixture. Homogeneous cloud formation is the predominant process if the cooling of the gas–vapour particles is so fast that the vapour pressure,

† Email address for correspondence: xsluo@hotmail.com

p_v, far exceeds its saturated value, p_{vs}, i.e. that the supersaturation, $S = p_v/p_{vs}$, becomes sufficiently high. Because the rate of droplet formation, the nucleation rate, exponentially depends on supersaturation, the number density of homogeneously formed droplets easily exceeds the density of condensation nuclei. Homogeneous cloud formation occurs and is studied in Laval nozzles (Adam & Schnerr 1997), in shock tubes (Barschdorff & Filippov 1970) and in expansion wave tubes (Holten, Labetski & van Dongen 2005), in expansion cloud chambers (Wölk & Strey 2001), in steam turbines (Petr, Kolovratnik & Hanzal 2003) and to some extent around airfoils in transonic flight (Rusak & Lee 2000; Lee & Rusak 2001; Li *et al.* 2005).

Condensation leads to the subsequent release of latent heat, which may have a strong impact on flow conditions. This was first reported by Prandtl (1936) for a supersonic nozzle flow of humid air at the Volta Congress in Rome. The presence of a so-called x-shock in an arc-shaped nozzle is caused by the condensation of water vapour. The phenomenon was later investigated extensively, both experimentally and theoretically. Surveys are given by Zierep (1969, 1990), Wegener (1975), Delale, Schnerr & van Dongen (2007) and Luo *et al.* (2007*a*).

The formation of shock waves in condensing nozzle flows is directly related to the release of latent heat. Adding heat to a supersonic flow leads to a deceleration and a corresponding compression of the flow particles. For increasing humidity, the compression disturbance develops into a steady shock wave upstream of the point of latent heat release. The structure of the shock depends on the shape of the nozzle. If the humidity of the gas is increased even more, a steady flow solution no longer exists and condensation-induced oscillations are found, characterized by the generation of unsteady shock waves (Adam & Schnerr 1997; Schnerr 2005).

This paper focuses on waves generated by condensation. A numerical study of condensation-induced waves for two different situations is shown. First, the response of the flow in a slender Laval nozzle to a discontinuous change in the humidity of the entering gas is considered. A sudden onset of condensation occurs, which leads to upstream- and downstream-moving shocks and to the start of flow oscillations. The different wave patterns observed will be compared with results of a Rayleigh–Bartlmä analysis (Bartlmä 1963, 1975), which combines the Rayleigh theory of heat addition with unsteady gasdynamics. The second problem studied is the onset of condensation in an unsteady rarefaction fan in humid nitrogen. As we will see, the onset of condensation again leads to upstream- and downstream-moving secondary shocks in agreement with the Rayleigh–Bartlmä analysis. Finally, the paper treats the changes in the structure of the expansion fan as a result of repeated interactions of condensation-induced weak shocks, with emphasis on the asymptotic behaviour as $t \to \infty$.

2. Physical and numerical models

The physical and numerical models on which this analysis is based have been extensively described by Luo *et al.* (2006) and Luo *et al.* (2007*b*). These models are briefly discussed here for completeness.

We focus on dilute mixtures of vapour and droplets in a carrier gas with typical maximum liquid mass fraction smaller than 0.02. The liquid mass fraction, g, is defined as the ratio of the mass of the liquid droplets and the mass of the mixture. Carrier gas and vapour have equal temperatures, which may differ from the temperature of the droplet cloud. Vapour and carrier gas are assumed to behave as calorically perfect gases. The vapour is sufficiently dilute to be far from its critical state. We also neglect

the volume occupied by the liquid phase (a good approximation for small wetness ($g \leqslant 0.1$)).

The fluid dynamical behaviour of the two-phase system of gas/vapour and droplets is described by the Euler equations, supplemented with conservation laws for the first four moment equations of the droplet size distribution function $f(r;\boldsymbol{x},t)\mathrm{d}r$, being the number density of particles with radius between r and $r+\mathrm{d}r$ at time t and position $\boldsymbol{x}$. The moment Q_n is defined as

$$\rho Q_n = \int_{r_b}^{\infty} r^n f \,\mathrm{d}r. \tag{2.1}$$

The third-order moment, Q_3, is directly related to the liquid mass fraction, g, by

$$g = (4\pi/3)\rho_l Q_3, \tag{2.2}$$

with ρ_l the density of the liquid. It was shown by Hill (1966) that the moment equations fully describe the droplet growth process, if the droplet growth rate is independent of the droplet size.

The governing equation for the complete system can be written in the vectorial form as

$$\frac{\partial \boldsymbol{U}}{\partial t} + \frac{\partial \boldsymbol{F}}{\partial x} + \frac{\partial \boldsymbol{G}}{\partial y} = \boldsymbol{S}, \tag{2.3}$$

where $\boldsymbol{U}$ is the vector of unknowns, $\boldsymbol{F}$ and $\boldsymbol{G}$ represent the convective fluxes in the x and y directions, respectively, and $\boldsymbol{S}$ is the source term:

$$\boldsymbol{U} = \begin{pmatrix} \rho \\ \rho u \\ \rho v \\ \rho E \\ \rho g \\ \rho Q_2 \\ \rho Q_1 \\ \rho Q_0 \end{pmatrix}, \quad \boldsymbol{F} = \begin{pmatrix} \rho u \\ \rho u^2 + p \\ \rho uv \\ (\rho E + p)u \\ \rho gu \\ \rho Q_2 u \\ \rho Q_1 u \\ \rho Q_0 u \end{pmatrix}, \quad \boldsymbol{G} = \begin{pmatrix} \rho v \\ \rho uv \\ \rho v^2 + p \\ (\rho E + p)v \\ \rho gv \\ \rho Q_2 v \\ \rho Q_1 v \\ \rho Q_0 v \end{pmatrix}, \tag{2.4}$$

$$\boldsymbol{S} = \begin{pmatrix} 0 \\ 0 \\ 0 \\ 0 \\ \dfrac{4}{3}\pi\rho_l\left(Jr^{*3} + 3\rho Q_2 \overline{\dfrac{\mathrm{d}r}{\mathrm{d}t}}\right) \\ Jr^{*2} + 2\rho Q_1 \overline{\dfrac{\mathrm{d}r}{\mathrm{d}t}} \\ Jr^{*} + \rho Q_0 \overline{\dfrac{\mathrm{d}r}{\mathrm{d}t}} \\ J \end{pmatrix},$$

where E is the total energy per unit mass of mixture, u and v are the velocity in the x and y directions, respectively. The critical droplet radius r^* depends on the

supersaturation, S: $r^* = 2\sigma v_{ml}/(RT \ln S)$, with surface tension, σ, molar liquid volume, v_{ml} and universal gas constant, R. The homogeneous nucleation rate, J, is evaluated with the *internally consistent classical nucleation theory* (ICCT) (Luijten 1998; Luijten, Peeters & van Dongen 1999). The averaged droplet growth rate, $\overline{\mathrm{d}r/\mathrm{d}t}$, follows from the explicit droplet growth formulation by (Gyarmathy 1982; Peeters, Luijten & van Dongen 2001). The temperature difference between the droplets and the surrounding gas has been taken into account by applying a wet bulb approximation. The surface tension of water implemented in the numerical method is based on an extrapolation of empirical data (Lamanna 2000).

On the basis of the fractional-step-method (Oran & Boris 1987), we split the governing equations in two parts: the homogeneous part without source terms and the inhomogeneous part with the source terms due to phase transition. Two numerical methods are used in this study.

2.1. *The ASCE2D method*

The homogeneous part is solved by applying the same method as used in VAS2D developed by Sun (1998) and Sun & Takayama (1999) for compressible flows. For the inhomogeneous part, the treatment by Mundinger (1994) and Prast (1997) is followed. The combination of the two methods has been developed into a new numerical method: ASCE2D (two-dimensional and axisymmetric adaptive solver for condensation and evaporation) (Luo *et al.* 2006). In this method, the governing equations have been discretized on an unstructured quadrilateral mesh that adapts to the time-dependent flow. The accuracy of the present numerical method and the influence of mesh adaptation on the convergence of the numerical results have been investigated by Luo (2004).

2.2. *The space–time CESE method*

The space–time conservation element and solution element (CESE) method, invented by Chang (1995), is adopted in order to obtain highly accurate numerical solutions for flow problems involving both strong and weak waves. The stiff source terms introduced by phase transition are treated implicitly by an iteration procedure proposed by Yu & Chang (1997). For a detailed description of the implementation of this method and the treatment of the source terms, the reader is referred to the paper by Luo *et al.* (2007*b*).

In this study, the two numerical methods, ASCE2D and CESE, are used in different situations. For the simulation of the condensation processes in nozzle flows, the ASCE2D method is employed. The one-dimensional CESE method is applied to simulate the condensing flows in rarefaction waves. Mesh convergence is briefly discussed in Appendix A.

3. Effects of heat addition to steady and unsteady flow

Considering the case of a dilute vapour in a carrier gas, the whole thermal process of condensation can be interpreted as heat addition to the inert carrier gas due to the condensation of vapour, which is the classical Rayleigh problem of heat added to a one-dimensional flow of a given Mach number. We shall restrict ourselves to a calorically perfect gas and follow closely the analysis as summarized by Zierep (1990). Details are given in Appendix B.

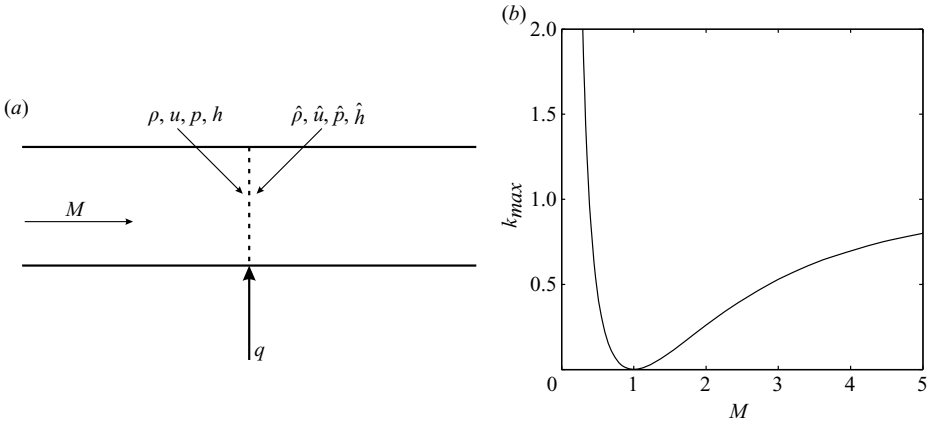

FIGURE 1. (*a*) The definition of the Rayleigh problem. (*b*) Maximum relative heat flow as a function of flow Mach number. $\gamma = 1.4$.

Let us assume a one-dimensional flow in positive x direction. At $x = 0$, a heat flow, q, is added to the flow per unit mass of mixture equal to

$$q = \kappa h_0 = \kappa \left(\tfrac{1}{2}u^2 + h\right), \tag{3.1}$$

in which the enthalpy, h, and the velocity, u, refer to the flow upstream of heat addition, see figure 1(*a*). The subscript '0' refers to isentropic stagnation conditions. By applying the conservations of mass, momentum and energy across the heat addition area, the solution to this problem is straightforward.

For a given flow Mach number, steady-state solutions are possible only for a limited range of the heat addition parameters: $\kappa \leqslant \kappa_{max}$, which is shown in figure 1(*b*). It is clear that at near sonic conditions, the capacity of the flow to absorb any heat in steady state becomes limited. This explains why for flows in slender nozzles, in which the release of latent heat may occur at a flow Mach number slightly above unity, this maximum value of κ is easily exceeded. In that case, a steady-state solution is not possible and the flow becomes periodic.

Waves generated by unsteady heat release have been considered in great detail by Bartlmä (1963, 1975) and Schnerr (2005). We shall apply the concepts, first described by Bartlmä, to a flow of a given Mach number, M_1, to which a constant heat flow of relative strength κ is added, starting at $t = 0$. Figure 2 gives an overview of the three different wave patterns to be expected and of the nomenclature of the different constant states. Details are given in Appendix B and can also be found in the survey by Delale *et al.* (2007). We shall briefly describe the three different regimes. For sufficiently low values of upstream flow Mach number M_1 and parameter κ, to be specified later, we observe an upstream-moving shock S_u, a downstream-moving shock S_d and a contact discontinuity, CD (regime *a*). An increase of M_1 leads to an increase of flow Mach number M_3 (see figure 2), until this flow Mach number becomes unity and thermal choking occurs. Then, an additional expansion fan (E) is necessary to satisfy the conservation laws (regime *b*). A further increase in M_1 leads to the disappearance of the left-running shock (regime *c*). In fact, the left-running shock then merges with the discontinuity caused by heat addition. In that case, the entrance flow is always supersonic.

The pressure and temperature profiles, obtained from numerical simulations (ASCE2D), for $\kappa = 0.1$ are also shown in figure 2 to facilitate the understanding of

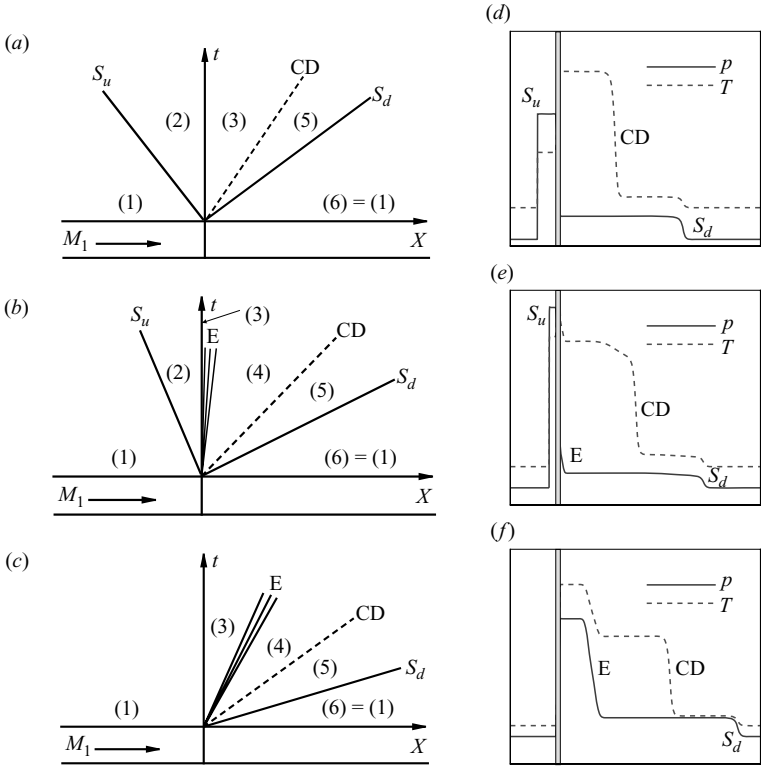

FIGURE 2. (*a–c*) Space–time diagrams of the wave pattern caused by onset of heat release. (*d–f*) Pressure and temperature profiles of the wave pattern by numerical simulation for $\kappa = 0.1$ and incoming flow Mach number 0.8, 1.1 and 1.6, respectively. S_u, upstream-moving shock wave; S_d, downstream-moving shock wave; E, expansion wave; CD, contact discontinuity. Heat is added in the shaded area.

the wave patterns. The incoming flow Mach numbers are 0.8, 1.1 and 1.6, respectively. The shaded area indicates where the heat is added. Figure 3 illustrates the pressure profiles for different incoming flow Mach numbers at the same time. The upstream-moving shock speed decreases (in this reference frame), while its strength increases with increasing incoming flow Mach number (see lines 1 and 2). When the incoming flow Mach number reaches a critical value, the upstream-moving shock and the heat addition discontinuity merge into one discontinuity at the plane of heat addition, $x = 0$ (see line 3). A further increase of the incoming flow Mach number will not change this situation, but will move the expansion fan more downstream (see line 4).

The strengths of upstream- and downstream-moving shocks in terms of relative pressure changes are illustrated in figure 4(*a*). Results are given as functions of M_1 for $\gamma = 1.4$ and for different κ: 0.01, 0.05 and 0.1. Above a limiting value of M_1, no upstream shock is possible (regime *c*). In general, the upstream-moving shock, if present, is stronger than the downstream-moving shock. For flow Mach numbers of about 0.5, the difference becomes quite significant. The larger the heat addition parameter κ, the stronger are both shock waves, and the larger the critical incoming flow Mach number. The solid curves represent a linearized solution of the conservation laws for heat addition as explained in Appendix B. The solution is remarkably accurate for both upstream and downstream shocks, except near $M_1 = 1$,

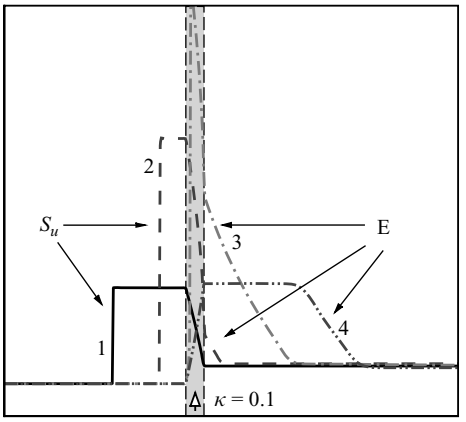

FIGURE 3. Pressure profiles for different incoming flow Mach numbers at the same moment. S_u, upstream moving shock; E, expansion wave. The shaded area indicates where the heat is added. $\kappa = 0.1$. Lines 1, 2 and 4 represent pressure profiles of wave patterns (a), (b) and (c), respectively. Line 3 illustrates the critical state between patterns (b) and (c).

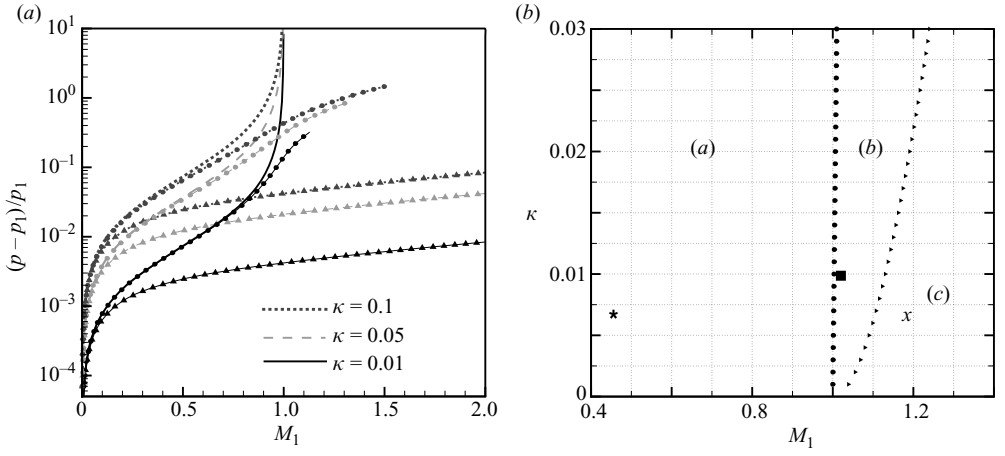

FIGURE 4. (a) Pressure ratios across upstream (circles) and downstream (triangles) shock waves. Lines: linear theory solutions for different κ. $\gamma = 1.4$. (b) Different regimes in the κ–M_1 plane.

where a singular behaviour is found, caused by the linearization. The different regimes can be mapped in a κ–M plane as shown in figure 4(b) for $\gamma = 1.4$.

4. The onset of condensation in a slender Laval nozzle

Detailed experimental and numerical studies on condensing flows in the slender supersonic nozzle G2 have been reported by Lamanna, van Poppel & van Dongen (2002) and Luo *et al.* (2006, 2007*a*). Here we focus on a simulation such that, first, a steady solution of dry nitrogen flow is obtained. Then, humid nitrogen is replacing dry nitrogen and a condensation process starts. The shape and the steady solution of a dry nitrogen flow in nozzle G2 are shown in figure 5. The stagnation conditions are $p_0 = 8.67 \times 10^4$ Pa, $T_0 = 296.6$ K.

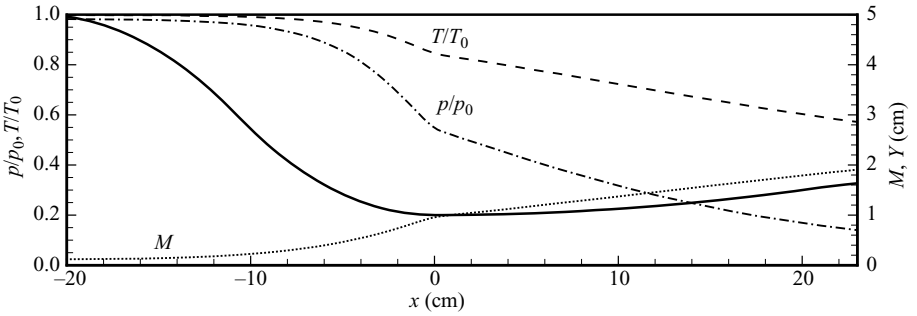

FIGURE 5. The shape of the supersonic nozzle G2 (solid line) and profiles of pressure (dash-dotted line), temperature (dashed line) and Mach number (dotted line) along the nozzle axis.

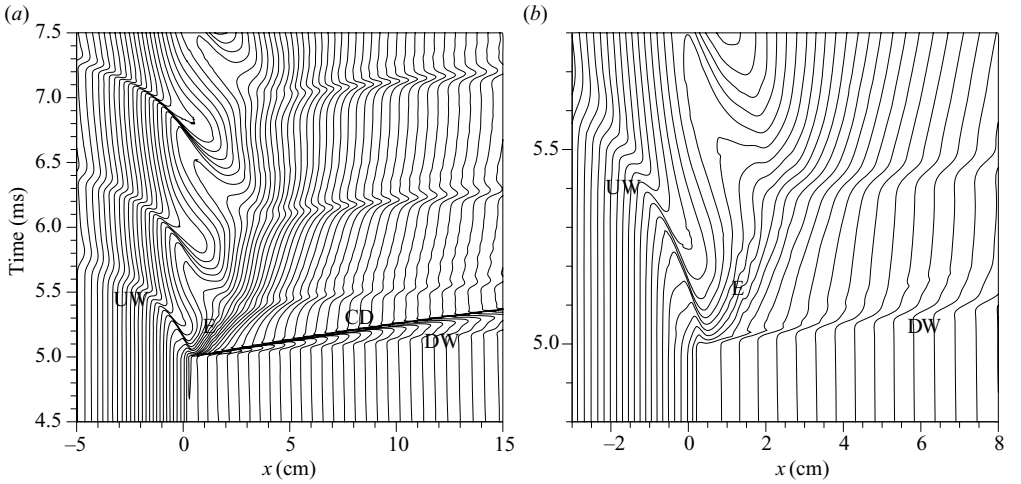

FIGURE 6. Numerical results for humid nitrogen flow with $S_{ini} = 0.517$ in nozzle G2 (ASCE2D): (*a*) iso-lines of density with an increment of 0.01 kg m^{-3}; (*b*) iso-lines of pressure with an increment of 1000 Pa in a space–time diagram, a close-up look near the onset point. After 5 ms, humid nitrogen starts to pass the nozzle throat, leading to condensation- and condensation-induced waves. After its initial stage, the condensation process becomes periodic. UW, upstream moving wave; DW, downstream moving wave; CD, contact discontinuity; E, expansion wave.

The initial saturation ratio of the humid nitrogen is $S_{ini} = 0.517$. Results are shown in the form of iso-density lines in a space–time diagram; see figure 6(*a*). The density range is from 0.21 to 0.97 kg m^{-3} with a contour increment of 0.01 kg m^{-3}. The densities are evaluated along the nozzle axis. We can estimate the position of the condensation onset from the two waves, which is approximately 3.6 mm downstream of the nozzle throat ($x_T = 0$), so that the Mach number at the onset of condensation is about 1.02. The value of the heat addition parameter due to condensation can be deduced from the liquid mass fraction and is about $\kappa = 0.01$. These onset conditions correspond with the square point in figure 4(*b*), so that wave pattern (*b*) is to be expected. From the iso-pressure lines of figure 6(*b*) (pressure increments 1000 Pa), the upstream- and downstream-moving waves induced by condensation can be recognized, the upstream-moving wave (UW) being clearly much stronger than the downstream one (DW), as predicted by the theory discussed before. By comparing the iso-density

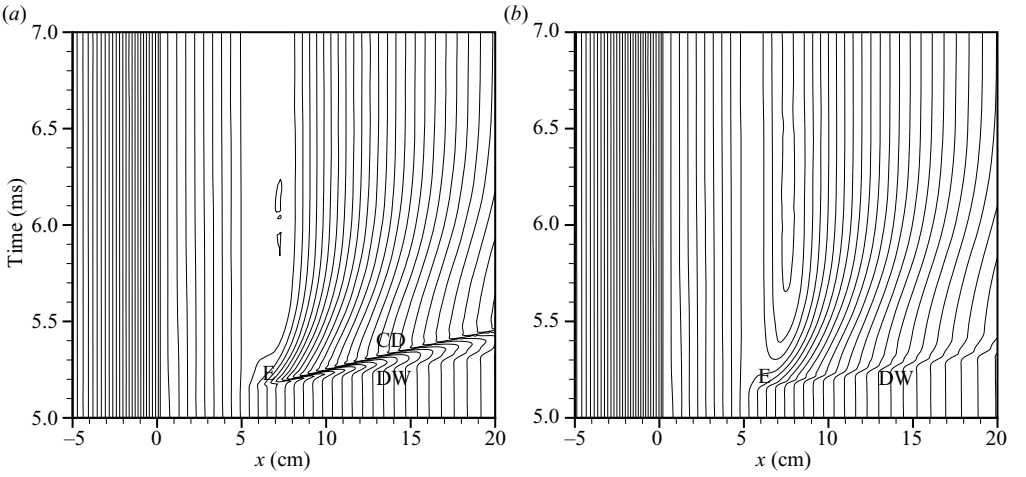

FIGURE 7. Numerical iso-lines of density with an increment of 0.01 $\mathrm{kg\,m^{-3}}$ (*a*) and pressure with an increment of 1000 Pa (*b*) in a space–time diagram for nitrogen flow in nozzle G2 (ASCE2D). After 5 ms, humid nitrogen starts to pass the nozzle throat, leading to condensation- and condensation-induced waves (regime *c*). After its initial stage, the condensation process becomes steady. Initial saturation ratio is $S_{ini} = 0.182$.

lines with the pressure lines, the contact surface (CD) and the expansion waves (E) can be identified typical for the wave pattern of regime (*b*). After the start of the condensation process, the flow becomes oscillatory. The point of onset of condensation shifts more downstream, while the local Mach number becomes subsonic. This implies a repeated wave pattern of regime (*a*) for the oscillation period, which can be directly found in figure 6.

If we reduce the humidity level (e.g. $S_{ini} = 0.182$ as shown in figure 7), the point of onset of condensation will shift downstream to a higher flow Mach number (e.g. 1.20 in figure 7). Then, we arrive in regime (*c*), observing a downstream moving shock only and the establishment of a steady condensing flow for flow conditions that approximately correspond to the cross-point in figure 4(*b*).

5. Homogeneous condensation in unsteady rarefaction waves, initial stage

It was observed, among others, by Sislian & Glass (1976) that cloud formation occurs in the rarefaction wave in a shock tube, when the driver section is filled with a humid gas. A numerical, analytical and experimental investigation of rarefaction waves in humid nitrogen was carried out by Smolders, Niessen & van Dongen (1989, 1992) and Smolders & van Dongen (1992). The nucleation process in their experiments was heterogeneous, because condensation nuclei, chromium oxide particles, were added to the gas. They also analysed the asymptotic behaviour of the expansion process as $t \to \infty$ to verify that the self-similar character, i.e. the x/t dependence of the wave, is restored asymptotically with the equilibrium speed of sound as the relevant scaling parameter (Smolders *et al.* 1992; van Dongen 2001). Homogeneous condensation in the expansion wave in a Ludwieg tube has been studied experimentally by Luo *et al.* (2007*a*). Their results have been compared with numerical simulations using the ASCE2D method (Luo *et al.* 2007*a*) and with simulations on the basis of the CESE method by Luo *et al.* (2007*b*). They reported repeated condensation phenomena due to the interaction of condensation-induced shock waves with the rarefaction front.

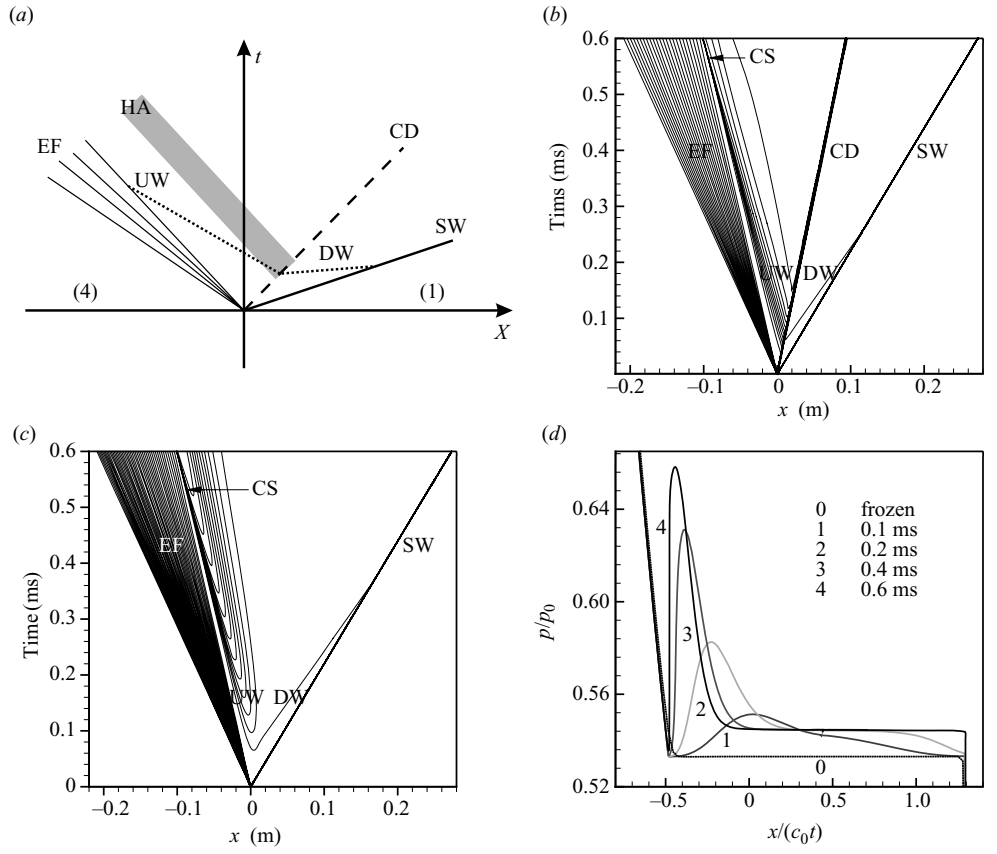

FIGURE 8. Shock tube problem in humid nitrogen. For initial state see the text. CESE method: (*a*) space–time diagram of shock tube problem. The shaded area (HA) indicates where heat release is to be expected. (*b*) Temperature contours with an increment of 2 K in space–time diagram. (*c*) Pressure contours with an increment of 1000 Pa in space–time diagram. (*d*) Snapshots of pressure as a function of reduced coordinate for different times in the initial stage. SW, shock wave; CD, contact discontinuity; EF, expansion fan; UW, upstream-moving wave; CS, condensation-induced shock wave; DW, downstream-moving wave.

Chirikhin (2007) numerically investigated the formation of a condensation shock in the high pressure section of a shock tube and found that in a fairly long channel, a periodic structure consisting of an alternating sequence of condensation shocks may be formed.

In this study, we consider the condensation phenomena in the high pressure section of a shock tube, filled with humid nitrogen. The numerical analysis is based on the ASCE2D method. The initial state (4) of the humid nitrogen in the high pressure section is $p_4 = 1$ bar, $S_{ini} = 0.82$, $T_4 = 295$ K. The initial state (1) in the low pressure section is dry nitrogen, $p_1 = 0.3$ bar, $T_1 = 295$ K. The wave pattern after removal of the diaphragm is shown in figure 8(*a*). A primary shock wave (SW) is running to the right into the low pressure section, an expansion fan or rarefaction fan (EF) is running to the left into the high pressure gas–vapour mixture. Because of the adiabatic cooling in the expansion fan, the gas becomes supersaturated and condensation occurs. The shaded area indicates where heat release is to be expected. Note that the locus of heat release moves with respect to the nitrogen flow with the local speed of sound in

good approximation. As a result of heat release, weak secondary shock waves will be generated according to the model discussed before (dashed lines, originating at the dashed contact surface). The left-running one is relatively strong and will overtake the characteristics of the expansion fan (see van Dongen *et al.* 2002 and Delale *et al.* 2007).

Temperature and pressure contours in the space–time diagram obtained with the numerical model (CESE) are shown in figure 8(*b, c*). It is quite clear that after some delay the heat addition due to condensation starts to affect the flow by generating a series of upstream-moving compression waves (UW), which eventually form a condensation induced shock (CS). The contours also show the presence of a downstream-moving shock, which interacts with the main shock. The combined upstream- and downstream-moving shock waves without an intermediate additional expansion fan can be characterized as wave pattern regime (*a*) of figure 2; see the asterisk point in figure 4(*b*). Snapshots of the pressure as a function of the reduced coordinate $x/(c_0t)$ at different times are depicted in figure 8(*d*) for the initial phase of the condensation process.

After the startup stage, the wave pattern continues to be affected by condensation. The condensation shock moves upstream, which leads to a temperature increase at the locus of the onset of nucleation. This is shown in figure 9, in which snapshots of pressure, p, temperature, T, supersaturation, S, and nucleation rate, Jn, are depicted as functions of the reduced coordinate $x/(c_0t)$. The shock wave causes nucleation to be quenched locally, which in turn weakens the shock strength. Far enough downstream of the condensation shock, a second zone of high supersaturation is formed and a renewed strong condensation takes place there, which leads to a second condensation shock moving upstream (see the supersaturation and nucleation rate curves of instants 4 and 5 in figure 9).

6. Homogeneous condensation in unsteady rarefaction waves, long-term behaviour

As pointed out in § 5, the condensation process in an unsteady expansion wave leads to additional unsteadiness, which is characterized by the formation and decay of condensation-induced weak shocks. This is illustrated in figure 10(*a*), in which the pressure as a function of time is shown for a fixed value of the reduced coordinate: $x/(c_0t) = -0.5$, which is inside the expansion wave at a locus where the different condensation induced waves can be clearly observed. The condensation process generates a 'delayed' and damped oscillation as time proceeds.

What we observe is a repeated process of new condensation-induced waves formed, which are 'absorbed' in the main expansion wave, thereby modifying its shape. It was shown in a previous study by Smolders & van Dongen (1992) for a simplified heterogeneous condensation model that the shape of the main expansion wave gradually changes to the solution to be expected on the basis of equilibrium gasdynamics for a wet gas–vapour mixture. The question is whether such behaviour will also be found for the much more complicated homogeneous nucleation and droplet growth process. Before we proceed with the numerical analysis, we shall first recall the non-trivial properties of an expansion fan in a two-phase mixture in phase equilibrium. Such a solution is characterized by wave splitting. This is caused by the peculiar behaviour of the equilibrium sound speed when passing the border between 'wet' and 'dry' for an isentropic change of the thermodynamic state. The reason is that the vapour mass fraction is constant as long as the mixture does not contain any

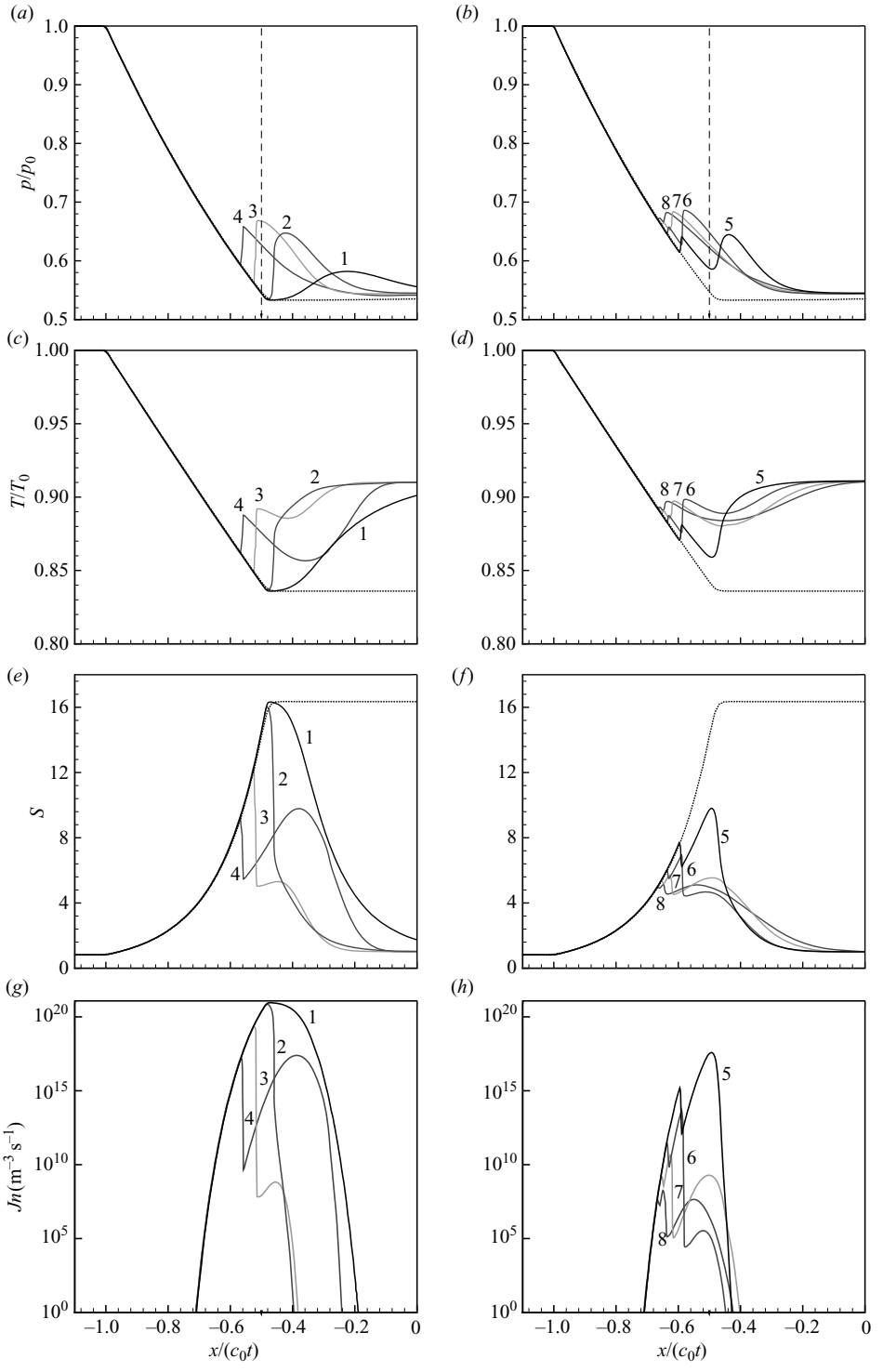

FIGURE 9. The development of the second condensation zone. Snapshots of pressure, temperature, saturation ratio and nucleation rate as functions of a reduced spatial coordinate at different times: 1, 0.2 ms; 2, 0.5 ms; 3, 1.0 ms; 4, 1.98 ms; 5, 4.998 ms; 6, 100 ms; 7, 1001 ms; 8, 10 010 ms. Dotted line represents the frozen value.

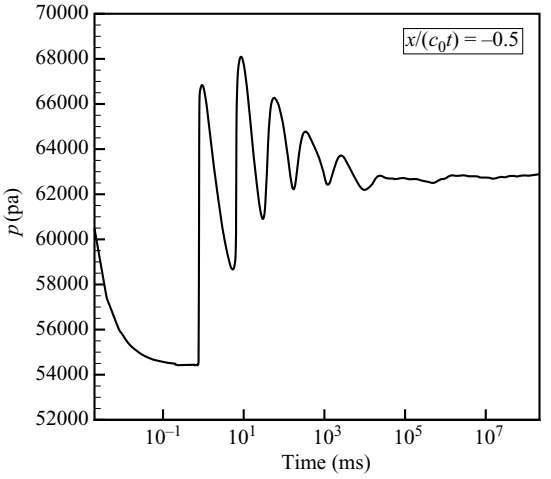

FIGURE 10. Pressure as a function of time at one fixed value of the reduced coordinate $x/(c_0 t) = -0.5$ with c_0 as the initial speed of sound in the driver section.

liquid, but that it is subjected to the Clausius–Clapeyron law in the presence of liquid. The equilibrium sound speed decreases approximately 10 % for the humid nitrogen mixtures studied at the passage from dry to wet. The equilibrium solution for the isentropic response to a discontinuous expansion is a similarity solution that follows from basic gasdynamics (Thompson 1972). Let us define the initial state at rest with pressure, p_0, and entropy, s_0. Then, for a left-running expansion fan the solution only is a function of (x/t) and can formally be written as follows:

$$x/t = u - c(p, s_0). \tag{6.1}$$

The Riemann invariant that holds for the whole domain is

$$u + \Gamma(p, s_0) = 0, \tag{6.2}$$

with the gasdynamic variable Γ defined as:

$$\Gamma(p, s_0) = \int_{p_0}^{p} \frac{1}{\rho(p, s_0) c(p, s_0)} \, \mathrm{d}p. \tag{6.3}$$

Equations (6.1)–(6.3) yield the velocity and pressure as a function of (x/t) for a given initial state and for a given equation of state for the gas–vapour mixture. Let us assume that the initial state is a dry one and that the expansion is sufficiently deep such that liquid is formed. At a certain state, indicated by subscript 'dw', the transition from dry to wet occurs. There the sound speed jumps from its dry value c_d to its lower wet value c_w. There is no reason why the velocity or the thermodynamic state would change. As a consequence, according to (6.1), a plateau of constant state, extending from $x/t = (u_{dw} - c_d)$ until $x/t \leqslant (u_{dw} - c_w)$, will separate the dry and wet part of the expansion fan. The procedure to solve the problem for a mixture of calorically perfect gases is given in Appendix C. Figure 11 shows the asymptotic solution for the pressure, p, the temperature, T, the liquid mass fraction, g, and the saturation ratio, S, as functions of the reduced coordinate $x/(c_0 t)$, together with the fully 'frozen' solution. Numerical results refer to four different instants of time. We recognize the first dry part of the expansion fan, the plateau of constant state separating the dry and wet part and the wet part of the wave in which the liquid mass fraction increases from 0

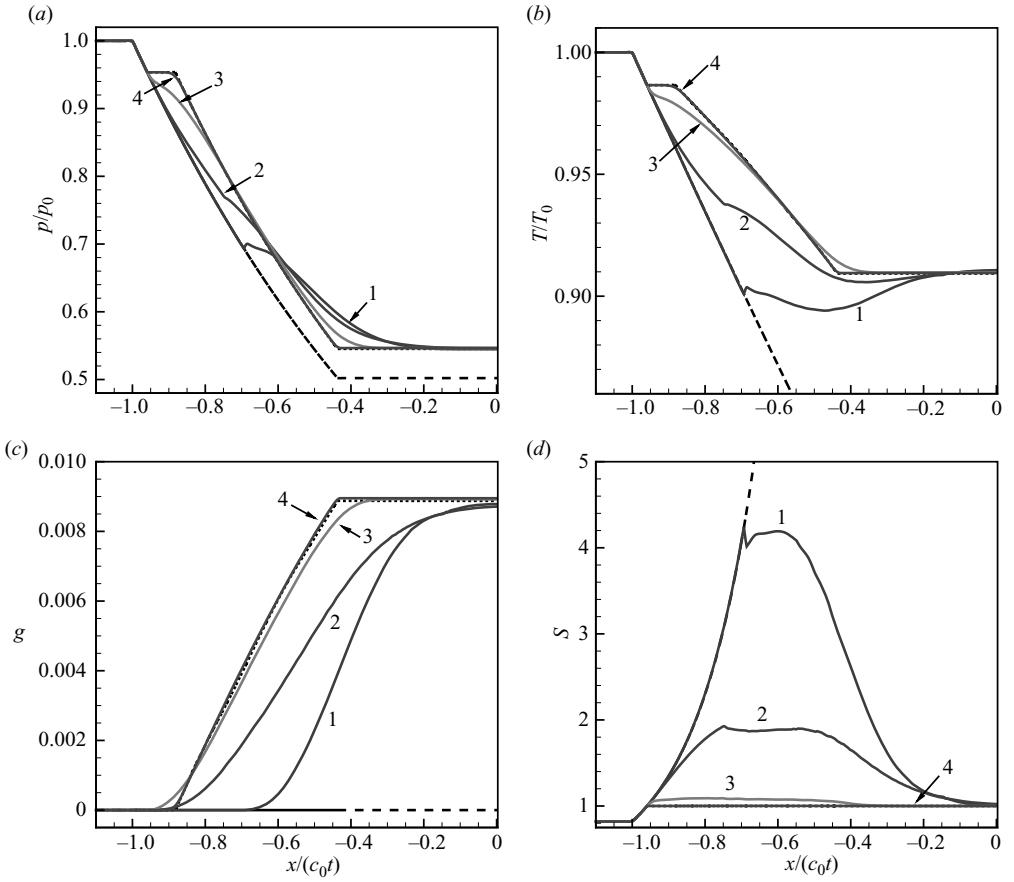

FIGURE 11. The unsteady expansion fan in humid nitrogen. Long-term behaviour. Numerical results (CESE, solid lines) for the pressure, temperature, liquid mass fraction and saturation ratio as functions of reduced coordinate at four different moments – 1, 2561 s; 2, 5.154×10^6 s; 3, 4.123×10^7 s; 4, 2.639×10^9 s. The dotted line denotes equilibrium solution with wet and dry parts, and the dashed line denotes frozen solution.

to its final value of 0.009. The pressure downstream the wave is not so much affected by condensation. Temperature (and density) certainly are significantly different. The temperature change after the passage of the wave in case of condensation is only half of its 'frozen' value. The saturation ratio shows relaxation towards unity in the wet part of the solution. It is clear that the numerical solution shows the expected asymptotic behaviour towards the phase equilibrium solution as $t \to \infty$.

7. Conclusions

Unsteady heat release due to the onset of nucleation and condensation in a quasi-one-dimensional flow leads to different types of wave patterns. We have found that these wave patterns can be qualitatively understood by means of a one-dimensional-model, originally proposed by Bartlmä, that combines the classical Rayleigh theory of heat addition with the gas dynamic laws for the different wave types involved. We have applied this model to the case of heat addition at a fixed plane, with strength κ, to a uniform flow of arbitrary Mach number. Three different regimes of wave patterns

have been found in the κ–M plane. The upstream-moving shock wave, if present at all, is much stronger than the downstream-moving wave in transonic flow. This explains why in the quasi-one-dimensional flow of a humid gas in a Laval nozzle only upstream-moving shocks have been observed. Linear theory gives accurate results for moderate heat addition, except near transonic conditions. The upstream motion of shock waves in a supersonic flow can only be explained with nonlinear theory.

A numerical analysis of the flow of nitrogen in a slender supersonic nozzle G2, in which dry nitrogen is replaced by humid nitrogen in a stepwise manner, has shown that the onset of condensation may lead to the complete wave pattern in terms of the Bartlmä analysis including both shock waves, the contact surface and the expansion fan. After the initial condensation process, the flow becomes oscillatory, with repeated upstream and downstream shocks, without an expansion fan. For a lower initial humidity, condensation occurs more downstream, at a higher flow Mach number, and as expected only a downstream-moving shock is observed.

The simple wave model for unsteady heat addition can also be used as an approximate description of the initial effects of condensation and latent heat release caused by a strong one-dimensional rarefaction fan in a humid gas. Because the condensation front follows the tail of the expansion wave with some delay, the relative flow Mach number of the condensation front is always close to unity. In our numerical analysis of the problem we could observe regime (a), upstream- and downstream-moving shocks in agreement with the unsteady heat addition model.

The structure of the expansion fan is modified by the condensation-induced waves. The upstream-moving shock even affects the local thermodynamic state such that the nucleation and condensation process is locally quenched. Far enough downstream of the condensation shock a second zone of high supersaturation is formed and a renewed strong condensation takes place there, which leads to a second condensation shock moving upstream. This process repeats and forms a 'delayed' and damped oscillation. This process has been analysed in terms of the approach to the full phase equilibrium solution. It was shown that the structure of such an equilibrium expansion wave is determined by the peculiar behaviour of the equilibrium sound speed, which jumps from its 'dry' value to its lower 'wet' value at the onset of liquid formation. As a consequence, the expansion fan shows a split structure and consists of a 'dry' part, a plateau of constant state and a 'wet' part. The full numerical solution of the problem appears to converge to the analytical equilibrium solution as $t \to \infty$. The results shown are particularly important for understanding the whole process of the interaction of condensation phenomena, condensation-induced waves and flows. They are not directly of practical value because of the large equilibration times involved. It would be interesting to extend the analysis to waves in pure vapours, with much higher nucleation rates.

This research was carried out with the support of the National Natural Science Foundation of China under grant 10776013 and the Open Foundation of the Key Laboratory of High Temperature Gas Dynamics (LHD), Chinese Academy of Sciences. Part of this research was carried out within the framework of the J. M. Burgerscentrum, Research School for Fluid Mechanics of the Netherlands.

Appendix A. Mesh study of simulation cases

Case 1. Condensing flows in the supersonic nozzle G2, ASCE2D method

Details on the numerical simulation of condensation in nozzle G2 with the ASCE2D

method, including a mesh study, are given by Luo (2004) and Luo *et al.* (2006). The mesh size adopted for the present work is about 2×2 mm^2 with an adaptation level of 4.

Case 2. Condensation in unsteady rarefaction waves, initial stage, CESE method
Condensing flow in shock tube has been studied by Luo *et al.* (2007*b*) and Cheng *et al.* (2010) using the CESE method, including the grid study. They concluded that the order of accuracy of the CESE method in computing the present problem in L1-norm is about 1.49. They also found that results with grid sizes of 0.05 mm and 0.025 mm do not show a visible difference in the shock shape. Based on this study, a grid size of 0.025 mm is chosen in this study.

Case 3. Condensation in unsteady rarefaction waves, long-term behaviour, CESE method
When long-term behaviour is considered, as time proceeds the source term's stiffness becomes weaker and a coarser grid can then be applied. To reduce the computing time, a changing grid size has been applied as suggested by Smolders *et al.* (1992). Specifically, after each 20 000 time steps, the grid size is doubled, which implies that the computational domain is doubled. The time step is also doubled in order to keep the CFL number constant throughout the calculation.

Appendix B. Rayleigh–Bartlmä theory for unsteady heat addition

We first consider the steady case as shown in figure 1(*a*) (Zierep 1990; Delale *et al.* 2007). Conservation of mass, momentum and energy connects the upstream state with the downstream state, indicated by a 'hat':

$$\hat{\rho}\hat{u} = \rho u, \;\; \hat{p} + \hat{\rho}\hat{u}^2 = p + \rho u^2, \tag{B 1}$$

$$\tfrac{1}{2}\hat{u}^2 + \hat{h} = \left(\tfrac{1}{2}u^2 + h\right)(1+\kappa), \tag{B 2}$$

where ρ and p are the gas density and the gas pressure, respectively. This leads to $p = \rho RT$ and $h = \gamma/(\gamma-1)RT$, where R is the gas constant, T is the gas temperature and γ is the specific heat ratio, to the following expressions:

$$I \equiv \sqrt{\left(\gamma + \frac{1}{M^2}\right)^2 - 2(\gamma+1)\left(\frac{1}{M^2} + \frac{\gamma-1}{2}\right)(1+\kappa)}, \tag{B 3}$$

$$\frac{\hat{u}}{u} = \frac{\rho}{\hat{\rho}} = F_u^{\pm}(M,\kappa) = \frac{1}{\gamma+1}\left(\gamma + \frac{1}{M^2} \pm I\right), \tag{B 4}$$

$$\frac{\hat{p}}{p} = F_p^{\pm}(M,\kappa) = \frac{M^2}{\gamma+1}\left(\gamma + \frac{1}{M^2} \mp \gamma I\right), \tag{B 5}$$

$$\hat{M} = F_m^{\pm}(M,\kappa) = \sqrt{\frac{\gamma + \frac{1}{M^2} \pm I}{\gamma + \frac{1}{M^2} \mp \gamma I}}. \tag{B 6}$$

In principle, there are two different branches of the solution, indicated by ($\pm$). They coincide if $I = 0$, which corresponds with the thermal choking condition, $\hat{M} = 1$. Solutions for finite κ in which the flow jumps from supersonic to subsonic (strong compression) or from subsonic to supersonic (strong expansion) are physically excluded (Landau & Lifshitz 1959). Consequently, only weak solutions exist with $\hat{M} = 1$ as limiting cases. In analogy with the theory of detonation, such a thermal

choking condition is sometimes referred to as a Chapman–Jouguet condensation discontinuity. Equation (B 3), with $I = 0$, yields directly the maximum heat addition possible, κ_{max}, for a flow of given Mach number:

$$\kappa_{max} = \frac{(1 - M^2)^2}{2(\gamma + 1)M^2 \left(1 + \dfrac{\gamma - 1}{2} M^2\right)}, \tag{B 7}$$

which is shown in figure 1(*b*). It will turn out to be useful to consider also the linearized solution of (B 1) and (B 2). It can easily be derived that

$$\frac{\hat{p} - p}{p} = \kappa \frac{\gamma M^2}{M^2 - 1} \frac{T_0}{T}, \tag{B 8}$$

$$\frac{\hat{u} - u}{c} = -\kappa \frac{M}{M^2 - 1} \frac{T_0}{T}. \tag{B 9}$$

It is clear that linearization always fails near sonic conditions.

Then we consider the unsteady case. Heat is added to a flow with Mach number M_1 at $x = 0$ in a compact manner so that the jump relations (B 1)–(B 6) apply for the transition at the plane of heat release $x = 0$. However, the condition upstream of the plane of heat release (state 2 in figure 2) is affected by the upstream-moving shock (if present), such that in general $M_2 \leqslant M_1$. Downstream of the plane of heat addition, a contact discontinuity separates states of different entropy (4) and (5), with equal pressures and velocities. We shall distinguish three different wave patterns as shown in figure 2.

Regime (a). Subsonic or transonic flow, $M_3 < 1$, no choking

If both $M_2 < 1$ and $M_3 < 1$, the different regimes are connected in a straightforward manner. States (1)–(2) and (5)–(6) are connected by ordinary shock relations, which are in fact given by the (–) branches of relations (B 3)–(B 6) for $\kappa = 0$. It should be realized that the Mach number in relations (B 3)–(B 6) then refers to the relative velocity between the wave and the gas in which the wave propagates. In this case, there is no expansion fan; see figure 2(*a*).

Regime (b). $M_3 = 1$, $M_2 < 1$, choking

For κ fixed and M_1 increasing, there will be a point at which the Mach number M_3 becomes unity: thermal choking. In that case, the upstream shock Mach number and the corresponding post-shock state, M_2, are fixed and are fully determined by the choking condition. We then need an additional wave to find a solution for the downstream shock strength: an expansion fan. In this case, the wave pattern is complete, as shown in figure 2(*b*). Because of the thermal choking, the leftmost characteristic line of the expansion fan coincides with the t axis, which implies that zone (3) is located at just downstream of the heat addition point, i.e. $x = 0^+$.

The additional equations connecting states (3) and (4) follow from the Riemann invariants for a left-running expansion fan and constant entropy (Courant & Friedrichs 1985):

$$u_3 + \frac{2c_3}{\gamma - 1} = u_4 + \frac{2c_3}{\gamma - 1}, \quad \frac{c_3}{c_4} = \left(\frac{p_3}{p_4}\right)^{\gamma - 1/2\gamma}. \tag{B 10}$$

The solution holds for supersonic flows, $M_1 > 1$, provided that the strength of the upstream shock is sufficient to move upstream. In this regime, the Mach number M_2 is always smaller than unity, the flow entering the plane of heat addition is subsonic. In the limiting case, in which the velocity of the upstream-moving shock has just become zero, the shock coincides with the heat addition jump for choked subsonic flow, which is identical with the 'choking' solution for supersonic flow.

Regime (c). $M_1 > 1$, $M_3 > 1$, supersonic, no choking, no upstream shock
If the flow Mach number M_1 is sufficiently large, there is no upstream disturbance and the flow decelerates to a fixed downstream Mach number $M_3 < M_1$, which leads to a compression. In order to match the post-shock conditions of the downstream shock, the expansion fan remains essential, and the actual wave diagram reduces to figure 2(*c*).

Appendix C. Equilibrium solution for a rarefaction fan

Consider a certain undersaturated mixture with pressure p_0, temperature T_0 and vapour fraction g_0, which is expanded isentropically, with entropy s_0, in a stepwise manner. From gasdynamics and the simple wave principle (Thompson 1972), a similarity solution for a left-running expansion fan reads:

$$x/t = u - c(p, s_0) = -\Gamma(p, s_0) - c(p, s_0), \tag{C 1}$$

with the gasdynamic variable Γ defined as

$$\Gamma = \int_{p_0}^{p} \frac{1}{\rho(p, s_0)c(p, s_0)}\,\mathrm{d}p. \tag{C 2}$$

Here c is the equilibrium sound speed. This is the implicit equation to be solved for c as a function of x/t. This is a very general solution that holds for any gas/vapour/liquid mixture in thermodynamic equilibrium. The formulation for a gas–vapour mixture is closed by specifying the thermodynamic properties of the gas–vapour–liquid mixture. We shall assume that gas and vapour behave calorically perfect with specific heats c_{pg}, c_{pv}, c_{vg}, c_{vv} with a constant specific heat of the liquid c_l and a linear dependence of latent heat on temperature $L = L_0 + (c_{pv} - c_l)T$.

For an undersaturated vapour, the vapour mass fraction is fixed and equals g_0 because the liquid mass fraction g is zero. For a wet mixture, p_v equals its saturation value, i.e. p_{vs}, which is a known function of temperature. In that case $g_0 - g = f(p, T)$. The next step is to consider the enthalpy of the mixture: $h = c_p T + (g_0 - g)L_0$. The mixture-specific heat is $c_p = (1 - g_0)c_{pg} + (g_0 - g)c_{pv} + gc_l$. The condition that the entropy is constant is equivalent to $\mathrm{d}h = 1/\rho \mathrm{d}p$. This gives a relation between $\mathrm{d}T$ and $\mathrm{d}p$:

$$\mathrm{d}T = \frac{1}{c_p \rho}\mathrm{d}p + \frac{L}{c_p}\mathrm{d}g. \tag{C 3}$$

Here $\mathrm{d}g$ denotes the change of liquid mass fraction, which is basically a function of T and p. The equation of state for the mixture is $p = \rho[(1 - g_0)R_g + (g_0 - g)R_v]T$. The 'dry' equilibrium sound speed follows from $c_d^2 = \gamma RT$, with $\gamma = c_p/(c_p - R)$, and $R = (1 - g_0)R_g + (g_0 - g)R_v$. The equilibrium sound speed for a wet mixture can be evaluated as

$$c_w^2 = c_d^2 \frac{[1 + \zeta^2(\gamma - 1)/\gamma - 1](p_{vs}/p)}{1 + (\gamma - 1)(\zeta - 1)^2(p_{vs}/p)}, \tag{C 4}$$

with $\zeta = L/(R_v T)$. In a formal sense, this is the complete solution. A consequence of the jump in sound speed is that a plateau of constant state is formed because the velocity u is continuous.

REFERENCES

Adam, S. & Schnerr, G. H. 1997 Instabilities and bifurcation of nonequilibrium two-phase flows. *J. Fluid Mech.* **348**, 1–28.

Barschdorff, D. & Filippov, G. A. 1970 Analysis of special conditions of the work of Laval nozzles with local heat supply. *Heat Trans. Sov. Res.* **2**, 76–87.

Bartlmä, F. 1963 Instationäre Strömungsvorgänge bei Uberschreiten der kritischen Wärmezufuhr. *Z. Flugwiss* **11**, 160–168.

Bartlmä, F. 1975 *Gasdynamik der Verbrennung*. Springer.

Chang, S. C. 1995 The method of space–time conservation element and solution element: a new approach for solving the Navier–Stokes and Euler equations. *J. Comput. Phys.* **119**, 295–324.

Cheng, W., Luo, X., Yang, J. & Wang, G. 2010 Numerical analysis of homogeneous condensation in rarefaction wave in a shock tube by the space–time CESE method. *Comput. Fluids* **39**, 294–300.

Chirikhin, A. V. 2007 Specific gasdynamical features of spontaneous condensation in an unsteady rarefaction wave. *Fluid Dyn.* **42** (1), 144–149.

Courant, R. & Friedrichs, K. O. 1985 *Supersonic Flow and Shock Waves*, 2nd edn. Springer.

Delale, C. F., Schnerr, G. H. & van Dongen, M. E. H. 2007 Condensation discontinuities and condensation induced shock waves. In *Shock Wave Science and Technology Reference Library,* Vol. 1*., Multiphase Flows*, pp. 187–230. Springer.

van Dongen, M. E. H. 2001 Wave propagation in multi-phase media. In *Handbook of Shock Waves*, pp. 741–781. Academic Press.

van Dongen, M. E. H., Luo, X., Lamanna, G. & van Kaathoven, D. J. 2002 On condensation induced shock waves. In *Proceedings of the 10th Chin. Symp. Shock Waves*, pp. 1–11. Chinese Academy of Science.

Gyarmathy, G. 1982 The spherical droplet in gaseous carrier streams: review and synthesis. In *Multiphase Science and Technology*, vol. 1, pp. 99–279. Springer.

Hill, P. G. 1966 Condensation of water vapour during supersonic expansion in nozzles. *J. Fluid Mech.* **25**, 593–620.

Holten, V., Labetski, D. G. & van Dongen, M. E. H. 2005 Homogeneous nucleation of water between 200 and 240 K: new wave tube data and estimation of the Tolman length. *J. Chem. Phys.* **123**, 104505.

Lamanna, G. 2000 On nucleation and droplet growth in condensing nozzle flows. PhD thesis, Eindhoven University of Technology.

Lamanna, G., van Poppel, J. & van Dongen, M. E. H. 2002 Experimental determination of droplet size and density field in condensing flows. *Exp. Fluids* **32**, 381–395.

Landau, L. D. & Lifshitz, E. M. 1959 *Fluid Mechanics*. Pergamom.

Lee, J. C. & Rusak, Z. 2001 Parametric investigation of nonadiabatic flow around airfoils. *Phys. Fluids* **13**, 315–323.

Li, L., Sun, X., Feng, Z. & Li, G. 2005 Transonic flow of moist air around an NACA0012 airfoil with non-equilibrium condensation. *Progr. Nat. Sci.* **15** (9), 838–842.

Luijten, C. C. M. 1998 Nucleation and droplet growth at high pressure. PhD thesis, Eindhoven University of Technology, Eindhoven, The Netherlands.

Luijten, C. C. M., Peeters, P. & van Dongen, M. E. H. 1999 Nucleation at high pressure. II. Wave tube data and analysis. *J. Chem. Phys.* **111**, 8535–8544.

Luo, X. 2004 Unsteady flows with phase transition. PhD thesis, Eindhoven University of Technology, Eindhoven, The Netherlands.

Luo, X., Lamanna, G., Holten, A. P. C. & van Dongen, M. E. H. 2007*a* Effects of homogeneous condensation in compressible flows: Ludwieg-tube experiments and simulations. *J. Fluid Mech.* **572**, 339–366.

Luo, X., Prast, B., van Dongen, M. E. H., Hoeijmakers, H. W. M. & Yang, J. 2006 On phase transition in compressible flows: modelling and validation. *J. Fluid Mech.* **548**, 403–430.

Luo, X., Wang, M., Yang, J. & Wang, G. 2007*b* The space–time CESE method applied to phase transition of water vapour in compressible flows. *Comput. Fluids* **36**, 1247–1258.

Mundinger, G. 1994 Numerische Simulation Instationärer Lavaldüsenströmungen mit Energiezufuhr durch Homogene Kondensation. PhD thesis, Universität Karlsruhe, Germany.

Oran, E. S. & Boris, J. P. 1987 *Numerical Simulation of Reactive Flow*. Elsevier.

Peeters, P., Luijten, C. C. M. & van Dongen, M. E. H. 2001 Transitional droplet growth and diffusion coefficients. *Intl J. Heat Mass Trans.* **44**, 181–193.

Petr, V., Kolovratnik, M. & Hanzal, V. 2003 Instrumentation and tests on droplet nucleation in LP steam turbines. *Power Plant Chem.* **5**, 389–395.

Prandtl 1936 *Atti del Convegno Volta*, 1st edn., vol. XIV. Reale Academia D'Italia.

Prast, B. 1997 Condensation in supersonic expansion flows: theory and numerical evaluation. Stan Ackermans Institute, Report I11, Eindhoven University of Technology, Eindhoven, The Netherlands.

Rusak, Z. & Lee, J. C. 2000 Transonic flow of moist air around a thin airfoil with nonequilibrium and homogeneous condensation. *J. Fluid Mech.* **403**, 173–199.

Schnerr, G. H. 2005 Unsteadiness in condensing flow: dynamics of internal flows with phase transition and application to turbomachinery. *Proc. IMechE,* Part C*: J. Mech. Engng Sci.* **219**, 1369–1410.

Sislian, J. P. & Glass, I. I. 1976 Condensation of water vapour in rarefaction waves: I. Homogeneous nucleation. *AIAA J.* **14** (12), 1731–1737.

Smolders, H. J. & van Dongen, M. E. H. 1992 Shock wave structure in a mixture of gas, vapour and droplets. *Shock Waves* **2** (4), 255–267.

Smolders, H. J., Niessen, E. M. J. & van Dongen, M. E. H. 1989 On the similarity character of an unsteady rarefaction wave in a gas–vapour mixture with condensation. In *IUTAM Symposium Göttingen/Germany* (ed. G. E. A. Meier & P. A. Thompson). Springer.

Smolders, H. J., Niessen, E. M. J. & van Dongen, M. E. H. 1992 The random choice method applied to nonlinear wave propagation in gas–vapour–droplets mixtures. *Comput. Fluids* **21** (1), 63–75.

Sun, M. 1998 Numerical and experimental studies of shock wave interaction with bodies. PhD thesis, Tohoku University, Sendai, Japan.

Sun, M. & Takayama, K. 1999 Conservative smoothing on an adaptive quadrilateral grid. *J. Comput. Phys.* **150**, 143–180.

Thompson, P. A. 1972 *Compressible Fluid Dynamics*. McGrow-Hill.

Wegener, P. P. 1975 Nonequilibrium flow with condensation. *Acta Mech.* **21**, 65–91.

Wölk, J. & Strey, R. 2001 Homogeneous nucleation of H_2O and D_2O in comparison: the isotope effect. *J. Phys. Chem.* B **105**, 11683–11701.

Yu, S. T. J. & Chang, S. C. 1997 Treatments of stiff source terms in conservation laws by the method of space–time conservation element/solution element. *AIAA Paper* 1997-0435.

Zierep, J. 1969 Schallnahe Strömungen mit Wärmezufuhr. *Acta Mech.* **8** (1–2), 126–132.

Zierep, J. 1990 *Strömungen mit Energiezufuhr*, 2nd edn. G. Braun.